Electronic Supplementary Material

Single-Ni-atoms on nitrogenated humic acid based porous carbon for CO_2 electroreduction

Delei Yu, Ying Chen, Yao Chen, Xiangchun Liu (✉), Xianwen Wei (✉), Ping Cui

Anhui Key Laboratory of Coal Clean Conversion & Utilization, School of Chemistry and Chemical Engineering, Anhui University of Technology, Ma'anshan 243002, China

E-mails: chunliu7@ahut.edu.cn (Liu X); xwwei@ahut.edu.cn (Wei X)

Inductively coupled plasma optical emission spectrometer measurement

Inductively coupled plasma optical emission spectrometer (ICP-OES, Agilent 720ES, USA) was employed to quantify the content of Ni.

Electrochemical measurement

The anode and cathode chambers were separated by a Nafion 117 membrane. The as-prepared catalysts (5 mg) were dispersed in a mixture of isopropanol (485 μL) and ultrapure water (485 μL) with 30 μL of Nafion solution (5 wt%). The above mixed solution was ultra-sonicated for 1 h to get a homogeneous catalyst ink. Then, 40 μL of each catalyst ink was drop-casted onto a carbon paper (1*1 cm^2), which was pre-dried at room temperature and acted as a working electrode. A Platinum sheet was used as a counter electrode, and an Ag/AgCl (3 M KCl) electrode was served as a reference electrode.

An aqueous solution of 0.1 M $KHCO_3$ was used as the electrolyte. A CO_2-saturated 0.1 M $KHCO_3$ solution was prepared by purging high-purity CO_2 into the cathodic compartment for 30 min, and a CO_2 flow rate of 25 mL/min was maintained during electrochemical measurements. The gas products were detected using online gas chromatograph (Agilent 7820, USA). The Faradaic efficiency of CO (FE_{CO}) can be calculated using

$$FE_{CO} = mnF/Q \quad \text{(S1)}$$

where m: the number of electrons required for the corresponding product (2 for CO); n: the number of moles of a specific product detected using GC; F: the Faraday

constant (96485.3 C/mol); and Q: the total charge passing through the working electrode.

The linear sweep voltammetry (LSV) curves were measured at a scan rate of 5 mV s^{-1} to obtain the polarization curves. The Tafel slope was calculated using the **Eq**. (S2)

$$\eta = b \log(j_{CO}/j_o) \quad \text{(S2)}$$

where η represents the overpotential; b is the Tafel slope; and j_{CO} and j_o are the partial current density for CO and the exchange current density, respectively.

Double-layer capacitance (C_{dl}) was the slope of the differences in the current-density variation obtained from the cyclic voltammetry (CV) curves at 0.6 V_{RHE} versus the scan rate (40, 80, 120, 160, and 200 mV s^{-1}) plot. C_{dl} was used to evaluate the electrochemical active surface area (ECSA) because it is proportional to the ECSA. The stability test of Ni-N-HAPC-950 was performed at −0.9 V_{RHE}. The electrochemical impedance spectroscopy (EIS) measurements were performed from 10^5 to 1 HZ at current density of 10 mA cm^{-2}.

Table S1 Ultimate analysis of HA (wt%)

Sample	Ultimate analysis/daf				
	C	H	N	S	O/diff.
HA	48.20	6.94	1.05	1.86	41.95

daf–dry ash-free basis; diff.: by difference

Table S2 Summary of catalytic performances of typical Ni-N-C catalysts in H-type electrolytic cells

Carbon material carrier or its precursor	Electrolyte	Catalytic performance	Ref.
4, 4′-Dipyridyl hydrate based porous carbon	0.1 M $KHCO_3$	FE_{CO}=82%, J_{CO}=11.2 mA cm^{-2} @ -0.75 V_{RHE}	[8]
Graphene	0.1 M $KHCO_3$	FE_{CO}=90%, J_{CO}=2 mA cm^{-2} @ -1.0 V_{RHE}; durability > 5 h @ -0.65 V_{RHE}; Tafel slope=126 mV dec^{-1}	[11]
Graphene nanosheets	0.5 M $KHCO_3$	FE_{CO}=95%, J_{CO}=11 mA cm^{-2} @ 620 mV; durability > 20 h @ 0.64 V; Tafel slope=110 mV dec^{-1}	[13]
Sodium citrate-based	0.5 M	FE_{CO}=96%, J_{CO}=2.8 mA cm^{-2}, durability > 7 h @ -0.6 V_{RHE}	[15]

carbon matrix	$KHCO_3$		
Graphene shell	0.1 M $KHCO_3$	FE_{CO}=93%, J_{CO}=4.0 mA cm^{-2}, durability > 20 h @ -0.82 V_{RHE}; Tafel slope=139 mV dec^{-1}	[19]
Carbon black	0.5 M $KHCO_3$	FE_{CO}=99%, J_{CO}=7.4 mA cm^{-2} @ -0.68 V_{RHE}; durability > 24 h @ -0.55 V; Tafel slope=101 mV dec^{-1}	[21]
Citric acid/melamine-based carbon material	0.5 M $KHCO_3$	FE_{CO}=95%, J_{CO}=5.5 mA cm^{-2}, durability > 25 h @ -0.75 V_{RHE}; Tafel slope=121 mV dec^{-1}	[R1]
MOF ZIF-8	0.5 M $KHCO_3$	FE_{CO}=72%, J_{CO}=10.5 mA cm^{-2} @ -0.89 V_{RHE}; durability > 60 h @ -1.0 V_{RHE}; Tafel slope=249 mV dec^{-1}	[R2]
MOF ZIF-8	0.5 M $KHCO_3$	FE_{CO}=95%, J_{CO}=6.6 mA cm^{-2}, durability > 10 h @ -0.65 V_{RHE}; Tafel slope=99 mV dec^{-1}	[R3]
Commercial multi-walled carbon nanotubes	0.1 M $KHCO_3$	FE_{CO}=91%, J_{CO}=7.2 mA cm^{-2}, durability > 10 h @ -0.8 V_{RHE}; Tafel slope=125 mV dec^{-1}	[R4]
o-phenylenediamine	0.5 M $KHCO_3$	FE_{CO}=93%, J_{CO}=3.9 mA cm^{-2}, durability > 12 h @ -0.67 V_{RHE}; Tafel slope=119 mV dec^{-1}	[R5]
Humic-acid-based porous carbon	0.1 M $KHCO_3$	FE_{CO}=92%, J_{CO}=6.9 mA cm^{-2}, durability > 8 h @ -0.9 V_{RHE}; Tafel slope= 123 mV dec^{-1}	This work

Table S3 Elemental composition from XPS analysis

Sample	Relative content/atomic %				Ni content/ wt%[a]
	C	N	O	Ni	
HA	52.58	1.9	45.52	0	-
HAPC	64.53	1.35	34.11	0	-
Ni-N-HAPC-850	75.28	4.89	19.15	0.68	-
Ni-N-HAPC-900	70.26	3.32	25.88	0.54	-
Ni-N-HAPC-950	67.15	2.93	29.50	0.42	3.87
Ni-N-HAPC-1000	68.22	2.48	28.82	0.48	-

[a] Determined from ICP-OES

Table S4 Summary of the curve-fitted peaks [38, 39]

Center (cm^{-1})	Symbol	Assignment
960–800	R	C–C on alkanes and cyclic alkanes; C–H on aromatic rings
1127–1082	S_R	C–H on aromatic rings; benzene (ortho-di-substituted)

		ring
1200–1185	S	$C_{aromatic}$–C_{alkyl}; aromatic (aliphatic) ethers; C–C on hydroaromatic rings; hexagonal diamond carbon sp^3; C–H on aromatic rings
1283–1255	S_L	Aryl–alkyl ether; para-aromatics
1323–1320	D	C–C between aromatic rings and aromatics with not less than 6 rings
1380–1378	V_R	Methyl group; semi-circle breathing of aromatic rings; amorphous carbon structures
1447–1440	V_L	Methylene or methyl; semi-circle breathing of aromatic rings; amorphous carbon structures
1521–1514	G_R	Aromatics with 3–5 rings; amorphous carbon structures
1598–1595	G	Graphite $E_{2g}{}^2$; aromatic ring quadrant breathing; alkene C=C
1730–1687	G_L	Carbonyl group C=O

Table S5 Crystalline structural parameters from XRD

	$(2\theta)_\gamma$/°	$(2\theta)_{002}$/°	β_{002}/°	d_{002}/nm	L_{002}/nm
HA	20.57	25.09	7.21	0.355	1.116
HAPC	21.12	25.46	5.61	0.350	1.435
Ni-N-HAPC-850	20.44	25.51	7.41	0.349	1.087
Ni-N-HAPC-900	21.87	25.60	7.26	0.348	1.109
Ni-N-HAPC-950	20.65	25.64	7.06	0.347	1.141
Ni-N-HAPC-1000	20.51	25.57	7.13	0.348	1.131

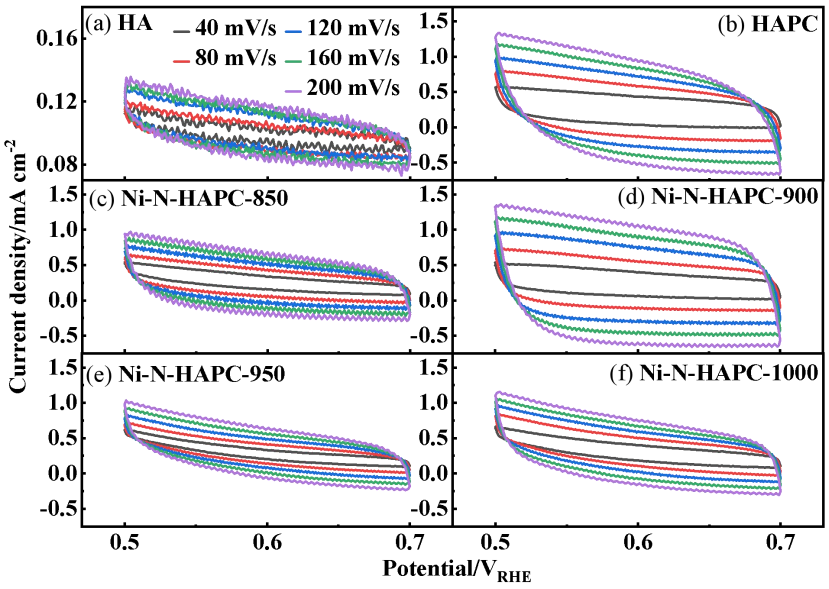

Fig. S1 Cyclic voltammograms for (a) HA, (b) HAPC, and (c-f) Ni-N-HAPC.

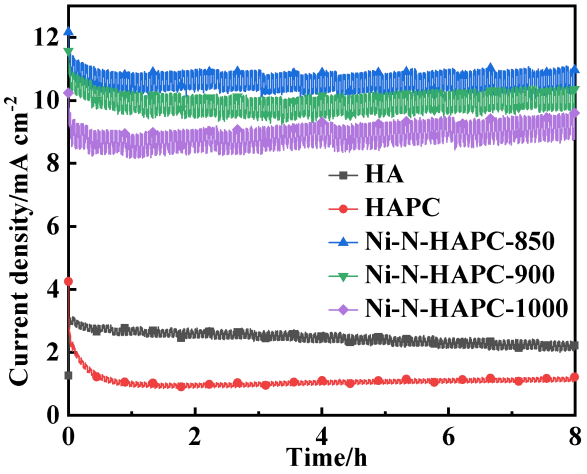

Fig. S2 Current–time responses of HA, HAPC, Ni-N-HAPC-850, Ni-N-HAPC-900, and Ni-N-HAPC-1000 for CO_2ER at −0.9 V_{RHE}.

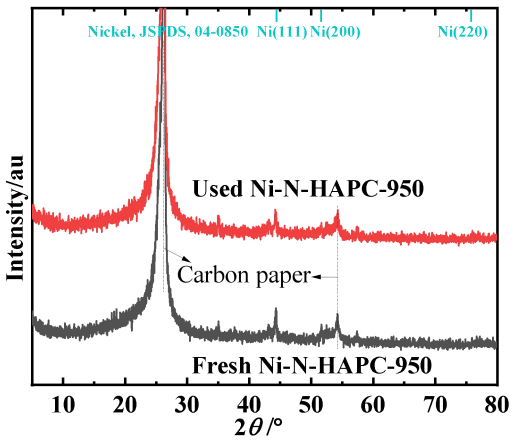

Fig. S3 XRD patterns of Ni-N-HAPC-950 before and after reaction.

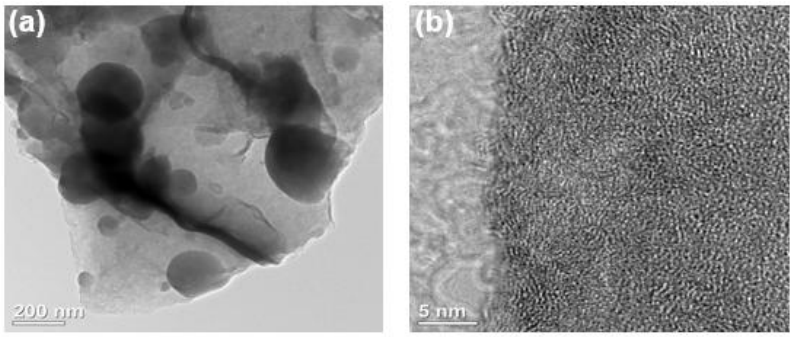

Fig. S4 (a) TEM and (b) HRTEM images of Ni-N-HAPC-950 after reaction.

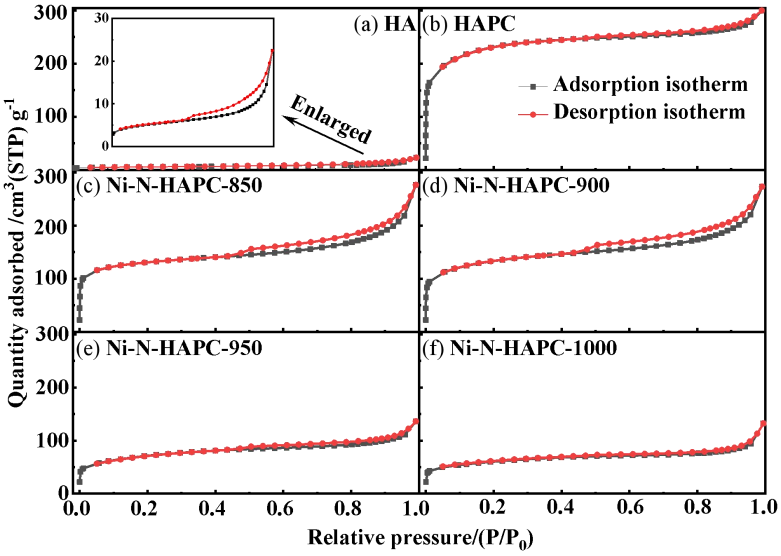

Fig. S5 N_2 adsorption-desorption isotherms of (a) HA, (b) HAPC, and (c-f) Ni-N-HAPC.

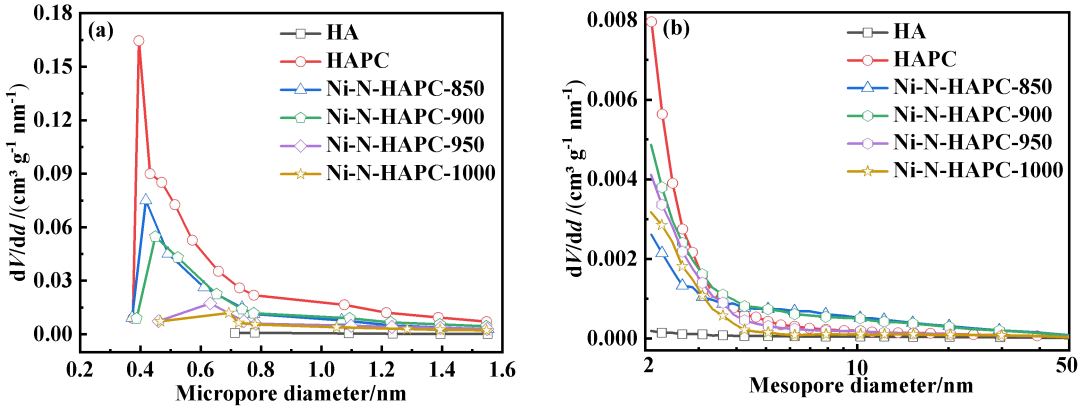

Fig. S6 (a) Micro- and (b) mesopore size distributions for all catalysts.

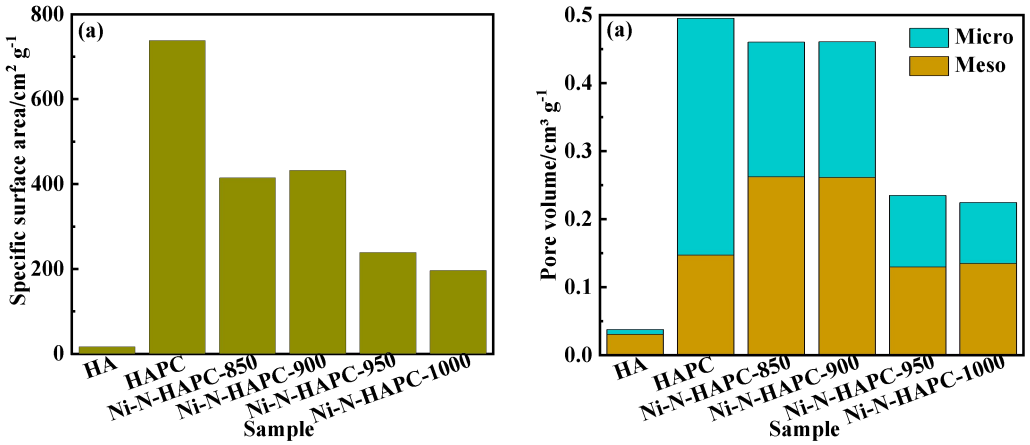

Fig. S7 (a) BET specific surface areas and (b) pore volumes for all catalysts.

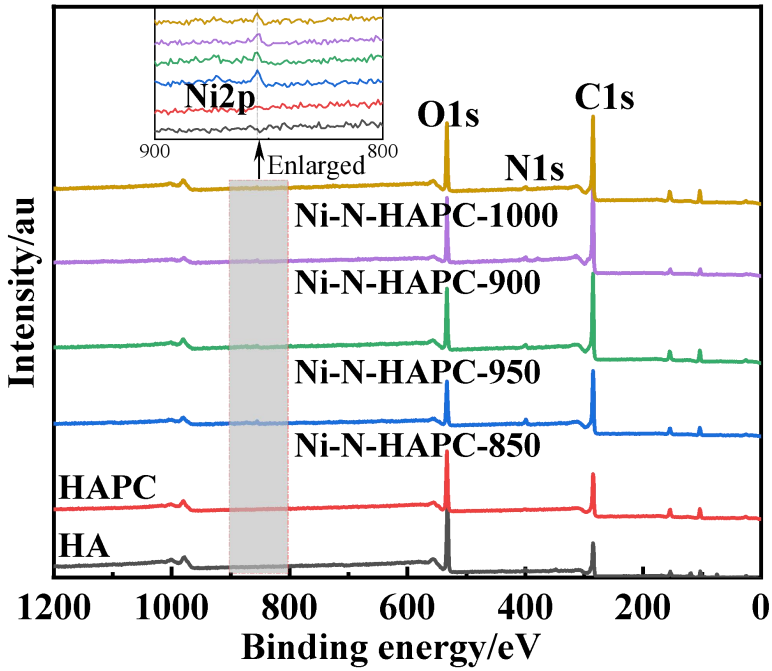

Fig. S8 XPS wide-survey spectra of HA, HAPC, and Ni-N-HAPC.

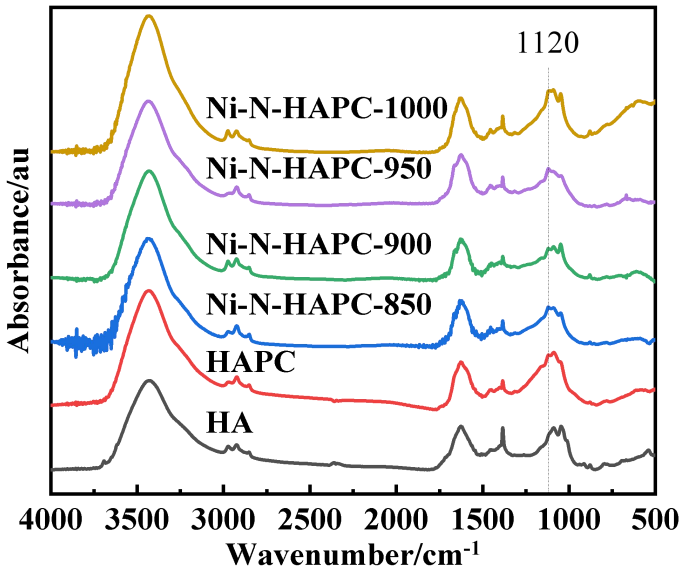

Fig. S9 FT-IR spectra of HA, HAPC, and Ni-N-HAPC.

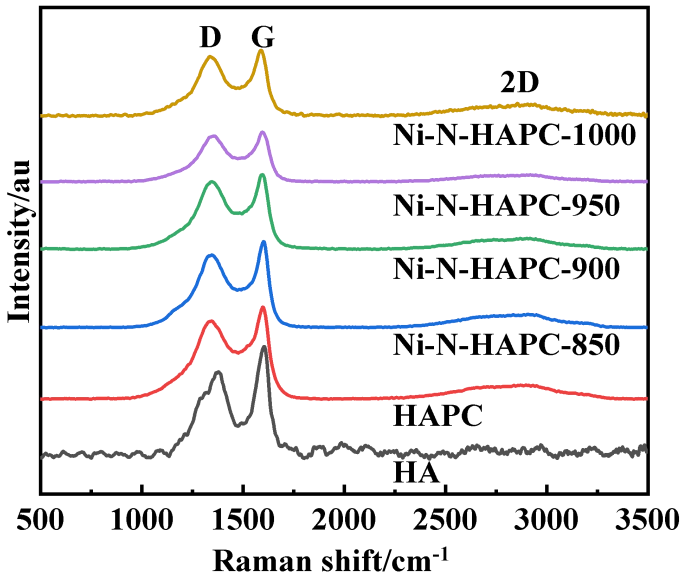

Fig. S10 Raman spectra for all catalysts.

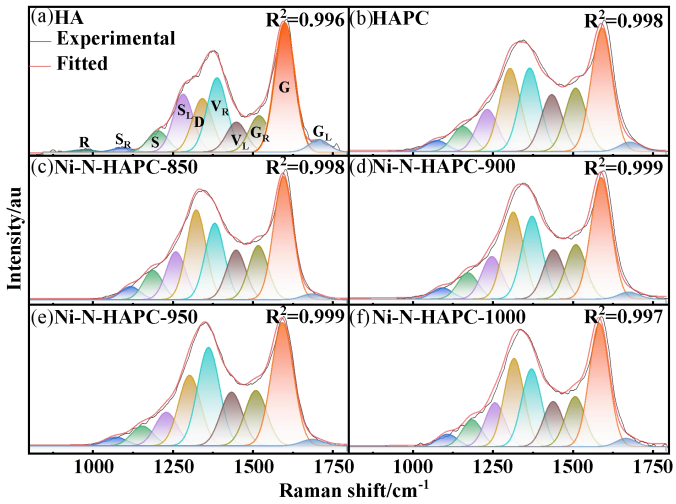

Fig. S11 Curve-fitted Raman spectra in the range of 1800–800 cm^{-1} for all catalysts ((a) HA, (b) HAPC, and (c-f) Ni-N-HAPC).

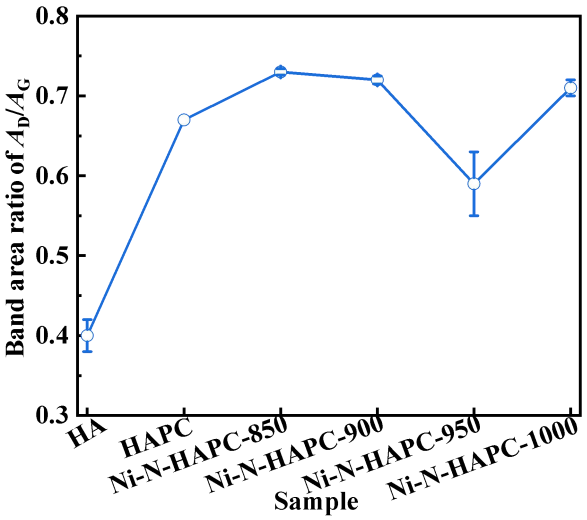

Fig. S12 A_D/A_G values for all catalysts.

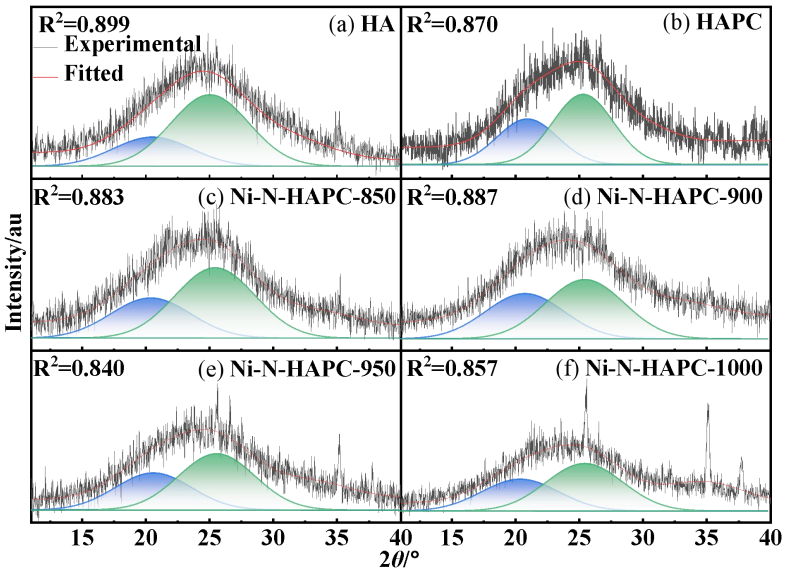

Fig. S13 Curve-fitted XRD patterns of (a) HA, (b) HAPC, and (c-f) Ni-N-HAPC.

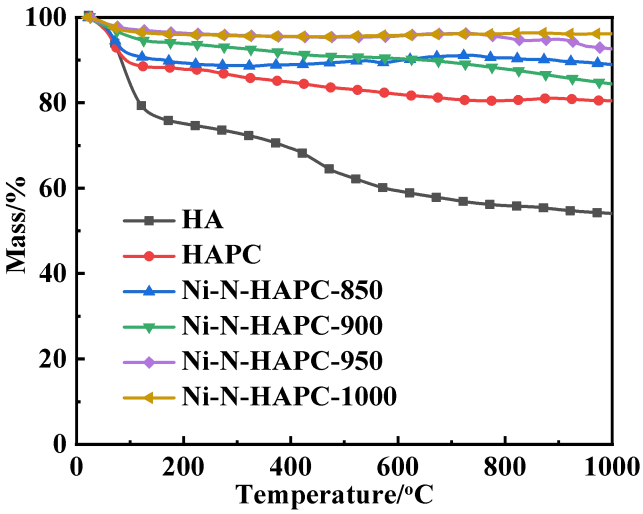

Fig. S14 Thermogravimetric (TG) curves of HA, HAPC, and Ni-N-HAPC.

References

R1. Ma Z, Zhang X, Wu D, Han X, Zhang L, Wang H, Xu F, Gao Z, Jiang K. Ni and nitrogen-codoped ultrathin carbon nanosheets with strong bonding sites for efficient CO_2 electrochemical reduction. Journal of Colloid and Interface Science, 2020, 570: 31-40.

R2. Zhao C, Dai X, Yao T, Chen W, Wang X, Wang J, Yang J, Wei S, Wu Y, Li Y. Ionic exchange of metal–organic frameworks to access single nickel sites for efficient electroreduction of CO_2. Journal of the American Chemical Society, 2017, 139(24): 8078-8081.

R3. Zhang Y, Jiao L, Yang W, Xie C, Jiang H L. Rational fabrication of low-coordinate single-atom Ni electrocatalysts by MOFs for highly selective CO_2 reduction. Angewandte Chemie International Edition, 2021, 60(14): 7607-7611.

R4. Fan Q, Hou P, Choi C, Wu T S, Hong S, Li F, Soo Y L, Kang P, Jung Y, Sun Z. Activation of Ni particles into single Ni–N atoms for efficient electrochemical reduction of CO_2. Advanced Energy Materials, 2020, 10(5): 1903068.

R5. Hu X M, Hval H H, Bjerglund E T, Dalgaard K J, Madsen M R, Pohl M M, Welter E, Lamagni P, Buhl K B, Bremholm M, et al. Selective CO_2 reduction to CO in water using earth-abundant metal and nitrogen-doped carbon electrocatalysts. ACS Catalysis, 2018, 8(7): 6255-6264.